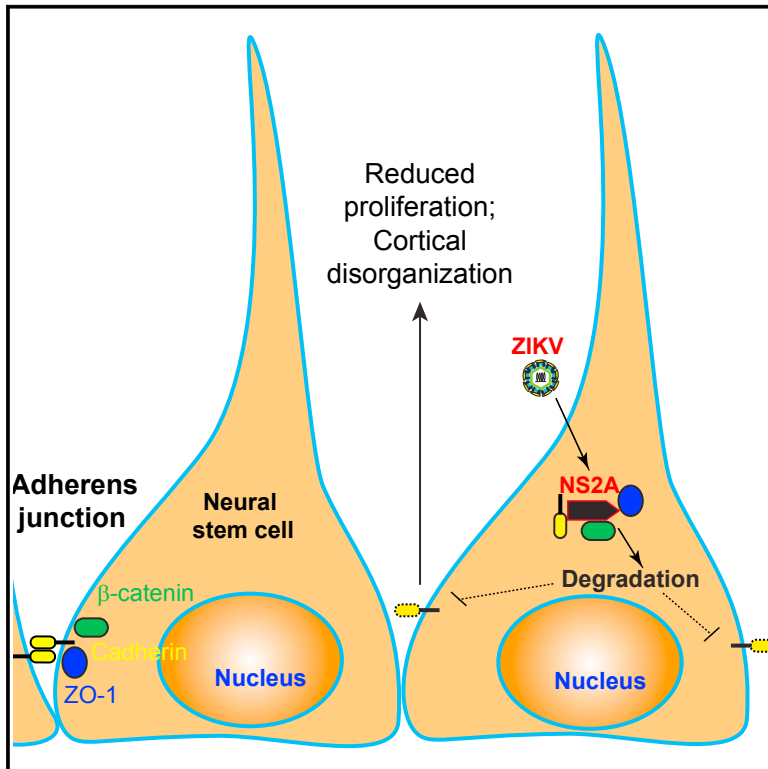


Cell Stem Cell

Zika-Virus-Encoded NS2A Disrupts Mammalian Cortical Neurogenesis by Degrading Adherens Junction Proteins

Graphical Abstract



Authors

Ki-Jun Yoon, Guang Song, Xuyu Qian, ..., Heng Zhu, Hongjun Song, Guo-li Ming

Correspondence

gming@mail.med.upenn.edu

In Brief

Zika virus infects neural stem cells and causes microcephaly. In this study, Yoon et al. showed that NS2A protein encoded by Zika virus, but not by Dengue virus, impairs proliferation of radial glial cells in both embryonic mouse cortex and human forebrain organoids. Mechanistically, ZIKV-NS2A disrupts adherens junction formation.

Highlights

- ZIKV-NS2A, but not DENV-NS2A, depletes RGCs in the embryonic mouse cortex
- ZIKV-NS2A expression causes mis-positioning of newborn neurons in the mouse cortex
- ZIKA-NS2A interacts with and depletes adherens junction (AJ) complex proteins
- ZIKV-NS2A impairs RGC proliferation and AJ formation in human forebrain organoids

Zika-Virus-Encoded NS2A Disrupts Mammalian Cortical Neurogenesis by Degrading Adherens Junction Proteins

Ki-Jun Yoon,^{1,2} Guang Song,³ Xuyu Qian,^{1,4} Jianbo Pan,⁵ Dan Xu,^{11,12} Hee-Sool Rho,³ Nam-Shik Kim,^{1,2} Christa Habela,² Lily Zheng,⁶ Fadi Jacob,^{1,7} Feiran Zhang,¹³ Emily M. Lee,¹⁶ Wei-Kai Huang,^{1,8} Francisca Rojas Ringeling,^{1,6} Caroline Viissers,^{1,9} Cui Li,¹¹ Ling Yuan,¹¹ Koeun Kang,¹ Sunghan Kim,¹ Junghoon Yeo,¹ Yichen Cheng,¹⁶ Sheng Liu,⁵ Zhexiong Wen,^{14,15} Cheng-Feng Qin,¹⁷ Qingfeng Wu,¹¹ Kimberly M. Christian,¹⁸ Hengli Tang,¹⁶ Peng Jin,¹³ Zhiheng Xu,¹¹ Jiang Qian,⁵ Heng Zhu,³ Hongjun Song,^{1,2,4,6,7,8,9,18,19,20} and Guo-li Ming^{1,2,4,7,8,9,10,18,19,21,*}

¹Institute for Cell Engineering

²Department of Neurology

³Department of Pharmacology and Molecular Sciences

⁴The Bioengineering Graduate Program

⁵Department of Ophthalmology

⁶The Human Genetic Pre-doctoral Program

⁷The Solomon H. Snyder Department of Neuroscience

⁸Graduate Program in Pathobiology

⁹The Biochemistry, Cellular and Molecular Biology Graduate Program

¹⁰Department of Psychiatry and Behavioral Sciences

Johns Hopkins University School of Medicine, Baltimore, MD 21205, USA

¹¹Institute of Genetics and Developmental Biology, Chinese Academy of Sciences, Beijing 100101, China

¹²College of Biological Science and Engineering, Institute of Life Sciences, Fuzhou University, Fuzhou 350116, China

¹³Department of Human Genetics

¹⁴Department of Psychiatry and Behavioral Sciences

¹⁵Department of Cell Biology

Emory University School of Medicine, Atlanta, GA 30322, USA

¹⁶Department of Biological Science, Florida State University, Tallahassee, FL 32306, USA

¹⁷Department of Virology, State Key Laboratory of Pathogen and Biosecurity, Beijing Institute of Microbiology and Epidemiology, Beijing 100071, China

¹⁸Department of Neuroscience, Mahoney Institute for Neurosciences

¹⁹Institute for Regenerative Medicine

²⁰The Epigenetics Institute

Perelman School for Medicine, University of Pennsylvania, Philadelphia, PA 19104, USA

²¹Lead Contact

*Correspondence: gming@mail.med.upenn.edu

<http://dx.doi.org/10.1016/j.stem.2017.07.014>

SUMMARY

Zika virus (ZIKV) directly infects neural progenitors and impairs their proliferation. How ZIKV interacts with the host molecular machinery to impact neurogenesis in vivo is not well understood. Here, by systematically introducing individual proteins encoded by ZIKV into the embryonic mouse cortex, we show that expression of ZIKV-NS2A, but not Dengue virus (DENV)-NS2A, leads to reduced proliferation and premature differentiation of radial glial cells and aberrant positioning of newborn neurons. Mechanistically, in vitro mapping of protein-interactomes and biochemical analysis suggest interactions between ZIKA-NS2A and multiple adherens junction complex (AJ) components. Functionally, ZIKV-NS2A, but not DENV-NS2A, destabilizes the AJ complex, resulting in impaired AJ formation and aberrant radial glial fiber scaffolding in the embryonic mouse cortex.

Similarly, ZIKA-NS2A, but not DENV-NS2A, reduces radial glial cell proliferation and causes AJ deficits in human forebrain organoids. Together, our results reveal pathogenic mechanisms underlying ZIKV infection in the developing mammalian brain.

INTRODUCTION

Zika virus (ZIKV) belongs to the *flavivirus* genus in the *Flaviviridae* family, which includes many significant pathogens, such as dengue virus (DENV), yellow fever virus, West Nile virus, and Japanese encephalitis virus (Lindenbach et al., 2007; Ming et al., 2016). In the wake of the recent ZIKV outbreak, the greatest concern has been the link between ZIKV infection during pregnancy and congenital neurodevelopmental birth defects, such as microcephaly (Rasmussen et al., 2016). Since the World Health Organization declared a Public Health Emergency of International Concern (Heymann et al., 2016), tremendous progress has been made in both clinical and basic ZIKV research

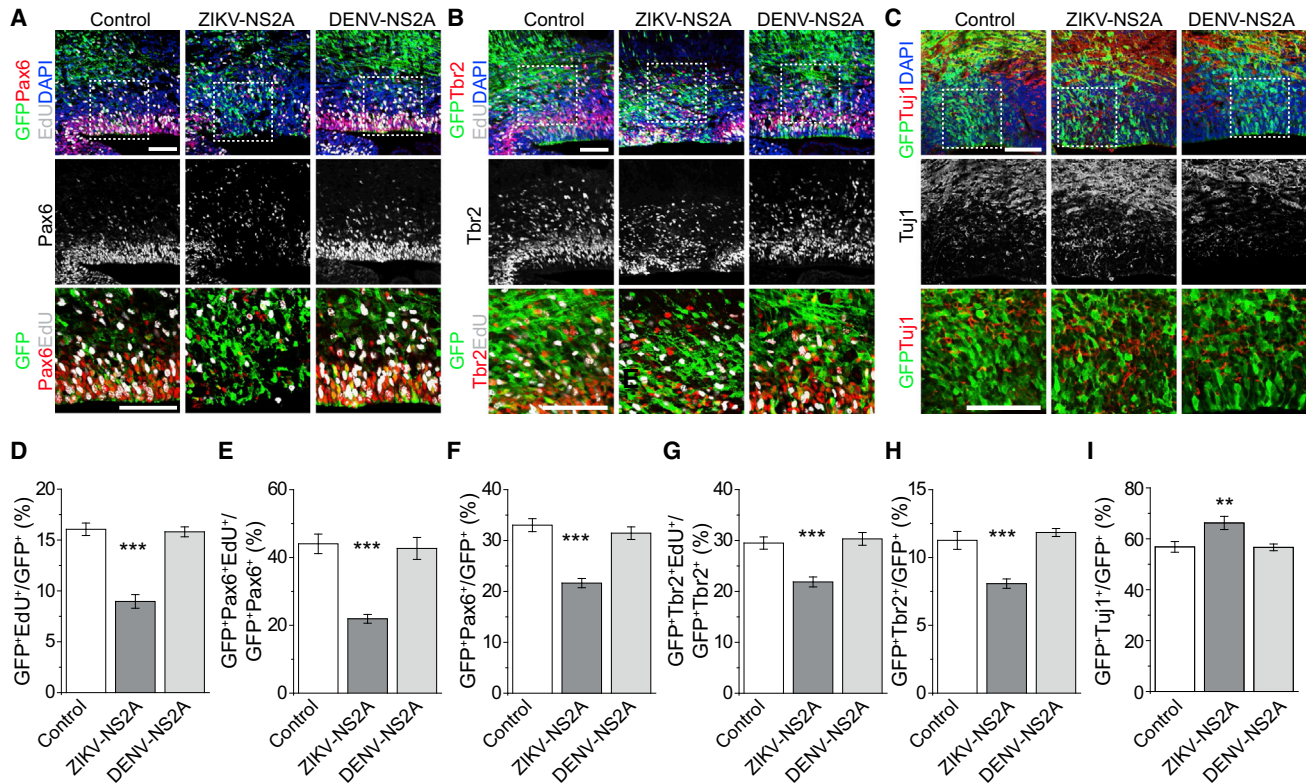


Figure 1. ZIKV-NS2A, but Not DENV-NS2A, Dysregulates Radial Glial Cells in the Embryonic Mouse Cortex

Embryonic mouse cortex was electroporated at E14.5 to express GFP, GFP and ZIKV-NS2A, or GFP and DENV-NS2A, followed by EdU labeling 2 hr before analysis at E17.5. Sample confocal images of immunostaining for Pax6 (A), Tbr2 (B), Tuj1 (C), and GFP and staining for EdU and DAPI are shown. The scale bars represent 100 μ m. The regions in white boxes (top panels) are shown at a higher magnification (bottom panels). Quantifications are also shown (D-I). Values represent mean \pm SEM (n = 5–7 sections from 3 or 4 animals; ***p < 0.001; **p < 0.01; one-way ANOVA). Also see [Figures S1](#) and [S2](#).

([Li et al., 2016b](#); [Ming et al., 2016](#)). ZIKV was found in microcephalic brains of fetuses from women infected with ZIKV during pregnancy ([Driggers et al., 2016](#); [Mlakar et al., 2016](#)), and ZIKV has been shown to directly infect cortical neural progenitors in various experimental model systems, including human induced pluripotent stem cell (iPSC)-derived and fetal-brain-tissue-derived neural progenitors in monolayer, 3D neurosphere, and brain organoid cultures and in mice ([Li et al., 2016b](#); [Ming et al., 2016](#)). At the cellular level, productive infection of neural progenitors by ZIKV delays cell cycle progression and increases cell death ([Ming et al., 2016](#)). At the molecular level, ZIKV infection leads to dysregulation of many signaling pathways ([Wen et al., 2017](#)). For example, ZIKV infection of human fetal neurospheres in culture inhibits the Akt-mTOR pathway, leading to defective neurogenesis and aberrant activation of autophagy ([Liang et al., 2016](#)). How ZIKV directly interacts with the host machinery to impact neurogenesis in the developing mammalian cortical cortex in vivo remains unknown.

The ZIKV genome consists of a positive-sense, single-stranded RNA approximately 11,000 nucleotides in length, encoding a single open reading frame (ORF) ([Garcia-Blanco et al., 2016](#)). Translation of the long ORF produces a large polyprotein with over 3,000 amino acid residues, which is then cleaved by both viral and host proteases to produce three structural proteins (C, prM, and E) and seven nonstructural proteins

(NS1, NS2A, NS2B, NS3, NS4A, NS4B, and NS5; [Figure S1A](#); [Garcia-Blanco et al., 2016](#)). Recent in vitro studies have shown that ZIKV-NS4A and ZIKV-NS4B inhibit neural progenitor growth ([Liang et al., 2016](#)). Here, we took an unbiased and systematic approach to screen for individual ZIKV protein components that may impact embryonic mouse cortical neurogenesis in vivo, followed by mechanistic analyses. We further extended our analysis to human embryonic cortical development using forebrain organoids derived from human iPSCs ([Qian et al., 2016](#)).

RESULTS

Reduced Proliferation and Premature Differentiation of Radial Glial Cells upon ZIKV-NS2A Expression in the Developing Mouse Cortex

We cloned each ORF of the ZIKV genome into an expression vector ([Table S1](#)) and co-expressed individual ZIKV proteins and GFP in embryonic day 14.5 (E14.5) embryonic mouse cortex via in utero electroporation ([Yoon et al., 2014](#)). For the initial screen, we pulsed animals with EdU at E17.5 for 2 hr and examined the percentage of EdU⁺ cells among GFP⁺Pax6⁺ radial glial cells (RGCs) as the proliferation index ([Figure S1B](#)). Among all ZIKV-encoded proteins, ZIKV-NS2A expression resulted in the most dramatic reduction in the proliferation index, whereas ZIKV-C had a mild effect ([Figures 1A](#) and [S1C](#)).

We next focused on ZIKV-NS2A for detailed analyses given that it produced the largest effect *in vivo*. ZIKV-NS2A exhibits 95.6%–99.9% identity at the protein level among different ZIKV strains, suggesting a highly conserved protein (Figure S2). Quantitative analysis showed that ZIKV-NS2A expression led to reductions in the percentage of EdU⁺ cells among all GFP⁺ cells and among GFP⁺Pax6⁺ RGCs compared to GFP expression alone, indicating deficits in RGC proliferation (Figures 1A, 1D, and 1E). In addition, the percentage of GFP⁺Pax6⁺ RGCs among all GFP⁺ cells was reduced upon expression of ZIKV-NS2A, suggesting depletion of RGCs in the developing mouse cortex (Figure 1F). RGCs give rise to Eomes (Tbr2)⁺ intermediate neural progenitor cells (IPCs), which differentiate into neurons (Götz and Huttnner, 2005). We found that ZIKV-NS2A expression also reduced percentages of EdU⁺ cells among GFP⁺Tbr2⁺ IPCs and of GFP⁺Tbr2⁺ IPCs among all GFP⁺ cells (Figures 1B, 1G, and 1H). These results are reminiscent of the impact of ZIKV infection on neurogenesis in the embryonic mouse cortex *in vivo* (Brault et al., 2016; Cugola et al., 2016; Li et al., 2016a; Wu et al., 2016). In addition to reduced proliferation of RGCs and IPCs, we also found a significant increase in the percentage of GFP⁺Tuj1⁺ immature neurons among all GFP⁺ cells, indicating premature differentiation of RGCs into neurons (Figures 1C and 1I), which is similar to a recent finding of the impact of direct ZIKV infection in cultured human neural progenitors and brain organoids (Gabriel et al., 2017).

DENV, a member of the *Flaviviridae* family closely related to ZIKV, has not been linked to either microcephaly or deficits in neural progenitor proliferation (Brault et al., 2016; Garcez et al., 2016). For comparison, we examined the functional outcome of DENV-NS2A expression. DENV-NS2A shares 24.8% identity at the protein level with ZIKV-NS2A (Figure S2) and presumably plays similar roles in viral replication and assembly for DENV. Upon *in utero* electroporation to express DENV-NS2A, we did not observe any significant differences in RGC and IPC proliferation or differentiation compared to GFP expression alone (Figure 1). Therefore, ZIKV-NS2A, but not DENV-NS2A, regulates radial glial neural stem cell properties in the embryonic mouse brain *in vivo*.

Aberrant Neuronal Positioning upon ZIKV-NS2A Expression in the Developing Mouse Cortex

To investigate the impact of ZIKV-NS2A expression on later processes of cortical development, we performed electroporation at E14.5 and examined cortical layer formation at E19.5. At this stage, the majority of transfected cells (GFP⁺) became SATB2⁺ upper layer neurons, whereas most early-born CTIP2⁺ lower layer neurons were GFP⁻ (Figure 2A). We found significant deficits in the positioning of GFP⁺SATB2⁺ neurons upon ZIKV-NS2A expression, many of which failed to migrate to the upper cortical layers and exhibited a much broader distribution (Figure 2). On the other hand, the early-born GFP⁻CTIP2⁺ neurons were largely unaffected (Figure 2). These results revealed that expression of ZIKV-NS2A during embryonic cortical development also disrupts positioning of newborn neurons and cortical layer organization *in vivo*.

Interaction between ZIKV-NS2A and Adherens Junction Complex Components

To investigate how ZIKV-NS2A directly interacts with the host protein machinery to impact neural stem cell behavior, we began

with an unbiased and systematic approach to generate testable hypotheses. We screened human proteins that can bind to recombinant ZIKV-NS2A protein or DENV-NS2A protein with protein microarray. Among 20,240 full-length recombinant human proteins spotted on the protein microarray (Jeong et al., 2012), which covers over 95% of protein-encoding genes in the human genome, 143 and 47 proteins were identified for ZIKV-NS2A and DENV-NS2A, respectively (Figure 3A; Table S2). A total of 45 proteins were shared between the two homologous NS2A proteins. Gene Ontology (GO) analysis of 143 ZIKV-NS2A interacting proteins revealed enrichment for multiple pathways, including extracellular exosome, cytoplasmic stress granule, and focal adhesion (Figure S3A; Table S3). Based on known protein-interaction networks, 83 ZIKV-NS2A interacting proteins can be visualized in a connected network ($p < 4.91 \times 10^{-13}$), whereas the remaining 60 proteins are singletons (Figure 3A; Table S4). Within the interaction network, 8 proteins (NME2, ARPC3, HSPB1, PABPC1, PTK2/FAK, VASP, PLEK, and SMAD7) have been reported to be related to cell adhesion ($p = 0.03$). Among singletons, NUMBL is also adhesion related (Rasin et al., 2007). Notably, 7 out of these 9 cell-adhesion-related proteins are ZIKV specific in this *in vitro* assay (Figures 3A and S3A).

The majority of these adhesion-related proteins (PTK2, VASP, NUMBL, SMAD7, and ARPC3) are linked to adherens junctions (AJ), which anchor RGCs and regulate their properties (Stocker and Chenn, 2015). To confirm that ZIKV-NS2A interacts with AJ complex components in a cellular context, we expressed ZIKV-NS2A in HEK293 cells and performed co-immunoprecipitation (coIP) analysis. Indeed, ZIKV-NS2A coIPed with multiple AJ components, including N-cadherin, ZO-1, β -catenin, SMAD7, NUMBL, and ARPC3 (Figure 3B). In contrast, these AJ components were not in the complex with DENV-NS2A (Figure 3B). SMAD7 was identified as an interactor of DENV-NS2A on the protein array, but not in the coIP analysis, which could be due to differences in the sensitivity of the two assays or differences in the biological context. We further confirmed the interaction of ZIKV-NS2A with multiple AJ complex components in cultured neural progenitors derived from E11.5 mouse cortex (Figure S3B).

Given that disruption of AJ formation in RGCs via a number of genetic manipulations all leads to premature differentiation and depletion of RGCs in the embryonic mouse cortex (Stocker and Chenn, 2015), which are the same phenotypes we observed for ZIKV-NS2A expression, these results from the *in vitro* screen raised the possibility that ZIKV-NS2A, but not DENV-NS2A, regulates AJ formation in RGCs *in vivo*.

Deficits in Adherens Junction Formation upon ZIKV-NS2A Expression

To test our hypothesis, we first examined the protein levels of AJ complex components upon ZIKV infection or NS2A expression. Direct ZIKV infection of mouse cortical neural progenitors led to reduced protein levels of several AJ components, including ZO-1, β -catenin, SMAD7, and NUMBL (Figures 4A and 4B). A similar reduction in these AJ components at the protein level was observed in mouse cortical neural progenitors expressing ZIKV-NS2A, but not DENV-NS2A (Figures 4A and 4B). The mRNA levels of most of these genes were not reduced upon ZIKV infection or ZIKV-NS2A expression, suggesting a

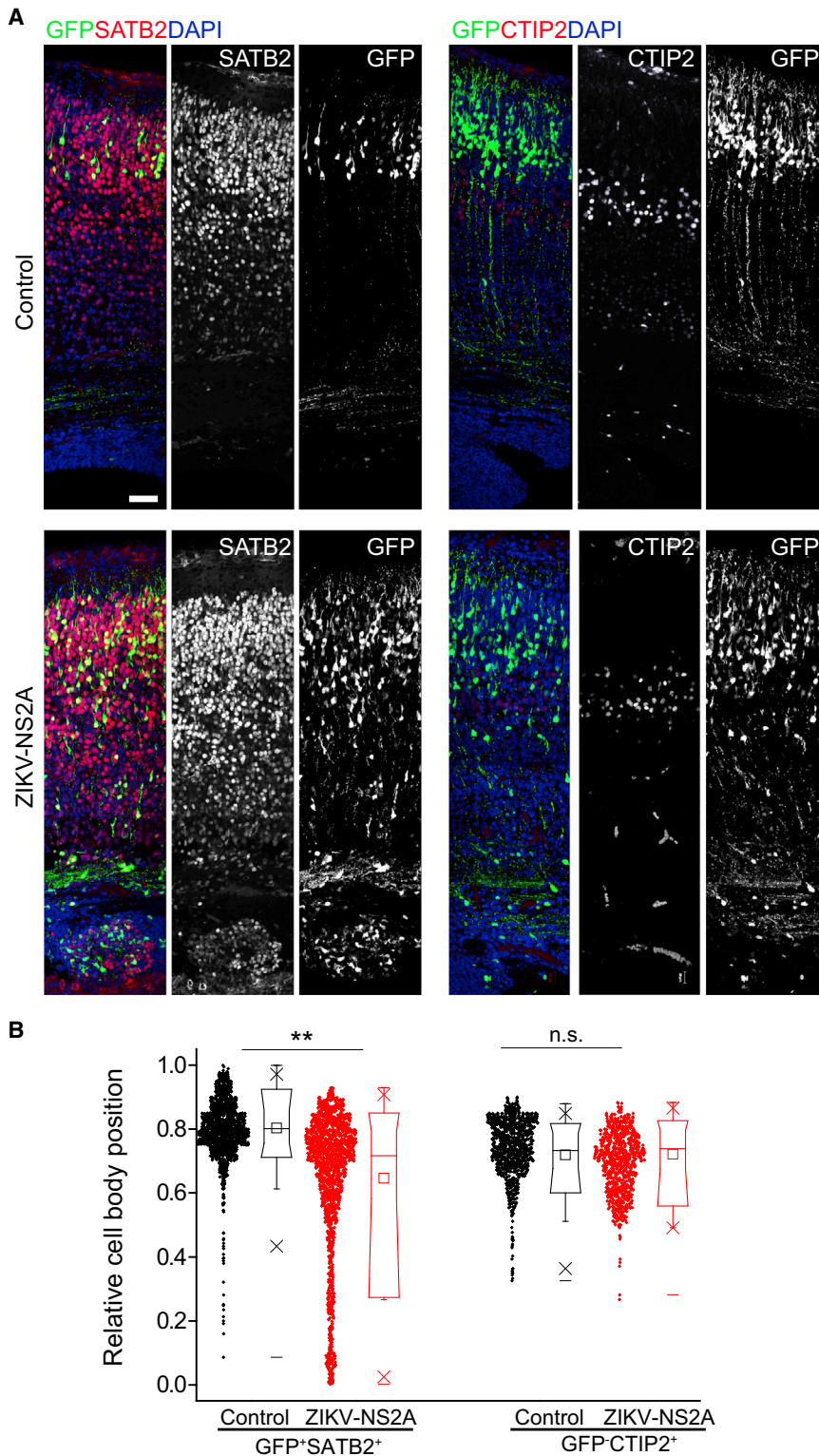


Figure 2. ZIKV-NS2A, but Not DENV-NS2A, Expression Leads to Aberrant Localization of Neurons in the Developing Mouse Cortex

(A) Embryonic mouse cortex was electroporated at E14.5 to express GFP, or GFP and ZIKV-NS2A, followed by analysis at E19.5. Sample confocal images of immunostaining for SATB2, CTIP2, and GFP and staining for DAPI are shown. The scale bar represents 50 μ m.

(B) Scatterplots and summary of cell body position of GFP⁺SATB2⁺ neurons and GFP⁺CTIP2⁺ neurons in the mouse cortex at E19.5. The distance of each cell to the apical surface was normalized to the total thickness of the neocortex. Each dot represents one neuron. The boxplots show the medians (line), means (square), interquartile ranges (box; 25%–75%), and extremes of the distribution (whisker; 99%: upper crosshatch; 1%: lower crosshatch; n = 8 sections from 4 animals for each condition; **p < 0.01; n.s. p > 0.1; Student's t test).

NS2A were co-localized with an ER marker calnexin (Figure S4C). In addition, levels of AJ complex components we tested were reduced in the fractionated ER preparation (Figure S4D). To explore cellular pathways that may degrade AJ complex components, we used a pharmacological approach. We found that ZIKV-NS2A-induced reduction of ZO-1 levels in HEK293 cells was prevented by bafilomycin A1 (BFA), an inhibitor for fusion of autophagosomes and lysosomes (Yoshimori et al., 1991), but not by proteasome inhibitors, MG-132, or delanzomib (Figures 4C and 4D). Furthermore, BFA treatment prevented ZIKV-NS2A-induced decreases of ZO-1 and NUMBL protein levels in mouse cortical neural progenitors (Figures 4E and 4F).

The above findings raised the possibility that interaction of ZIKV-NS2A with AJ complex components may lead to their depletion, resulting in deficits in AJ formation in RGCs. Indeed, immunostaining and quantification of β -catenin, PKC λ , or ZO-1 expression revealed significant deficits in AJ formation by RGCs upon expression of ZIKV-NS2A, but not DENV-NS2A (Figures 5A and 5B). Reduction of ZO-1 expression in Pax6⁺ and Nestin⁺ RGCs (Figures S5A and S5B) suggests that AJ deficits induced by

post-transcriptional regulatory mechanism (Figures S4A and S4B). It is known that some AJ components are pre-assembled in the endoplasmic reticulum (ER) before they are delivered to the cell membrane to form AJs (Chen et al., 1999). As expected, immunostaining showed that some ZIKV-NS2A and DENV-

ZIKV-NS2A occur prior to the depletion and premature differentiation of RGCs (Figures 1F and 1I). ZIKV-NS2A expression also led to disorganized radial glia fiber scaffolding and ventricular protrusions (Figures 5A, S5C, and S5D). Given that newborn neurons migrate along radial fibers of RGCs during

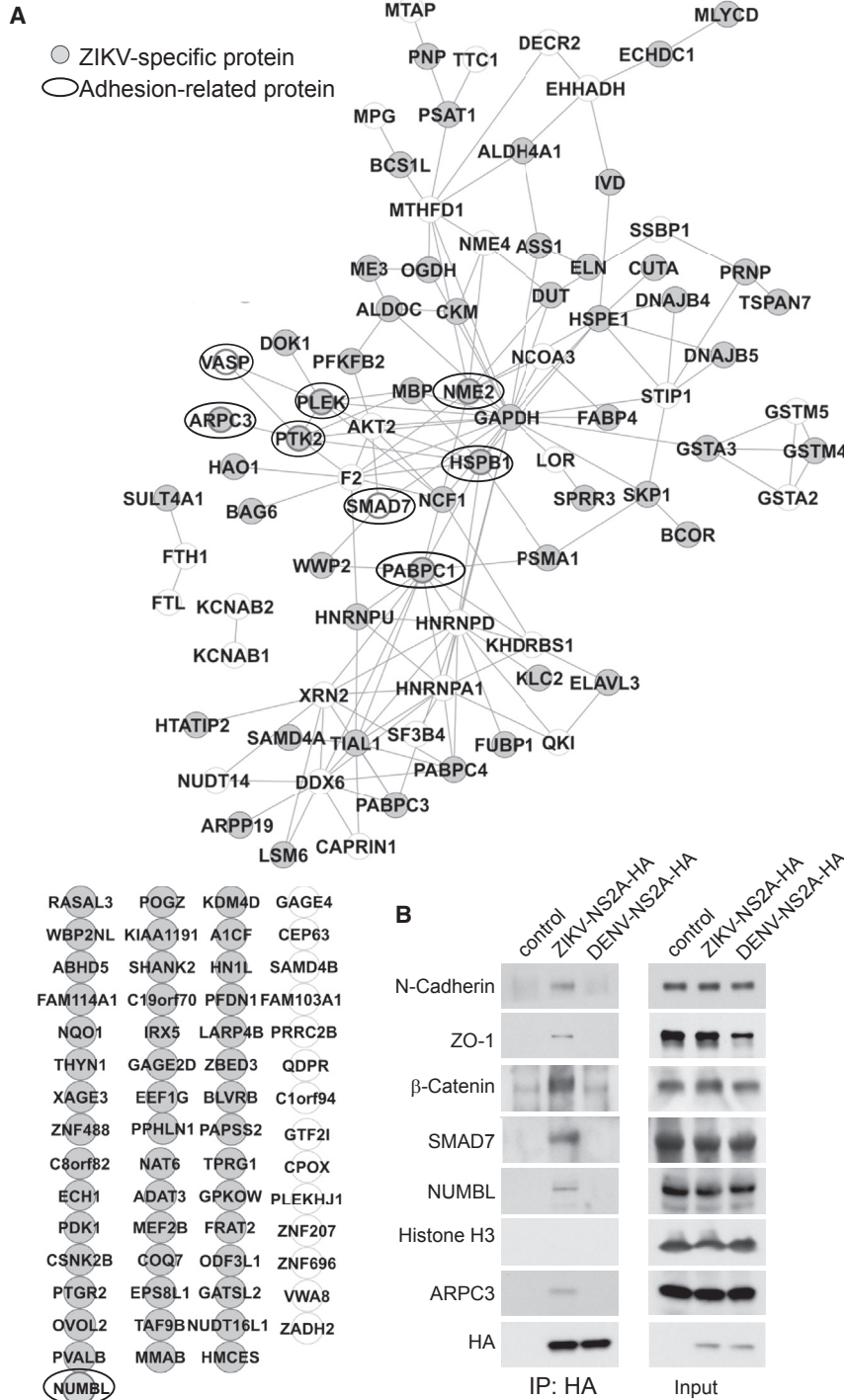


Figure 3. Protein-Protein Interactomes of ZIKV-NS2A and DENV-NS2A across the Human Proteome

(A) 143 and 47 direct ZIKV-NS2A and DENV-NS2A interacting proteins were identified in vitro using a protein array containing 20,240 full-length human proteins. Among 143 ZIKV-NS2A interacting proteins, 83 proteins can be visualized in a connected network based on existing literatures ($p < 4.91 \times 10^{-13}$, STRING analysis), whereas the remaining 60 proteins are singletons. ZIKV-NS2A-specific interacting proteins are coded in gray, and adhesion-related proteins are highlighted with circles. (B) Sample western blot images of colP analysis of HEK293 cells expressing GFP, ZIKV-NS2A and GFP, or DENV and GFP and analyzed for adherens junction complex components. Histone H3 served as a negative control for colP. Also see Figure S3.

E18.5 (Figures 5C and 5D) and ventricular protrusions at P3 (Figures 5C and S5E). Together, these results provide evidence that ZIKV infection and ZIKV-NS2A expression result in similar deficits of AJ formation of RGCs in the embryonic mouse cortex.

Deficits in Human Cortical Neurogenesis upon ZIKV-NS2A Expression

Finally, to determine whether ZIKV-NS2A dysregulates embryonic human cortical neurogenesis, we used the recently established human iPSC-derived forebrain organoid model (Qian et al., 2016; Xu et al., 2016). We co-expressed GFP and ZIKV-NS2A, or DENV-NS2A, in ventricular RGCs in day 45 forebrain organoids by electroporation and 3 days later pulsed with EdU (10 μ M) for 1 hr (Figure S6A). Expression of ZIKV-NS2A, but not DENV-NS2A, resulted in reduced percentages of EdU⁺ cells among all GFP⁺ cells and GFP⁺PAX6⁺ cells and of Ki67⁺ cells among all GFP⁺ cells within the ventricular structures compared to GFP expression alone (Figures 6A, S6B, and S6C). Furthermore, immunostaining and quantification of PKC λ expression revealed disrupted AJ formation in

embryonic cortical development (Buchman and Tsai, 2007), this deficit may contribute to aberrant cortical layer formation (Figure 2).

Next, we compared the impact of ZIKV-NS2A expression in RGCs to direct ZIKV infection of the embryonic mouse cortex. Following direct injection of the ZIKV-SZ strain (Li et al., 2016a) into the lateral ventricle of E13.5 mouse brain in utero, we observed deficits in AJ formation and radial fiber scaffolding at

ZIKV-NS2A-expressing regions at the ventricular surface (Figure 6B).

We observed some disruption of ventricular organization upon expression of ZIKV-NS2A, but not DENV-NS2A, at day 3 (45+3; Figure S6B) and more dramatically at day 7 (Figure 6C). Quantitative analysis showed a significantly increased percentage of GFP⁺PAX6⁺ cells that lost their radial morphology and instead exhibited multipolar morphology (Figure 6C). These

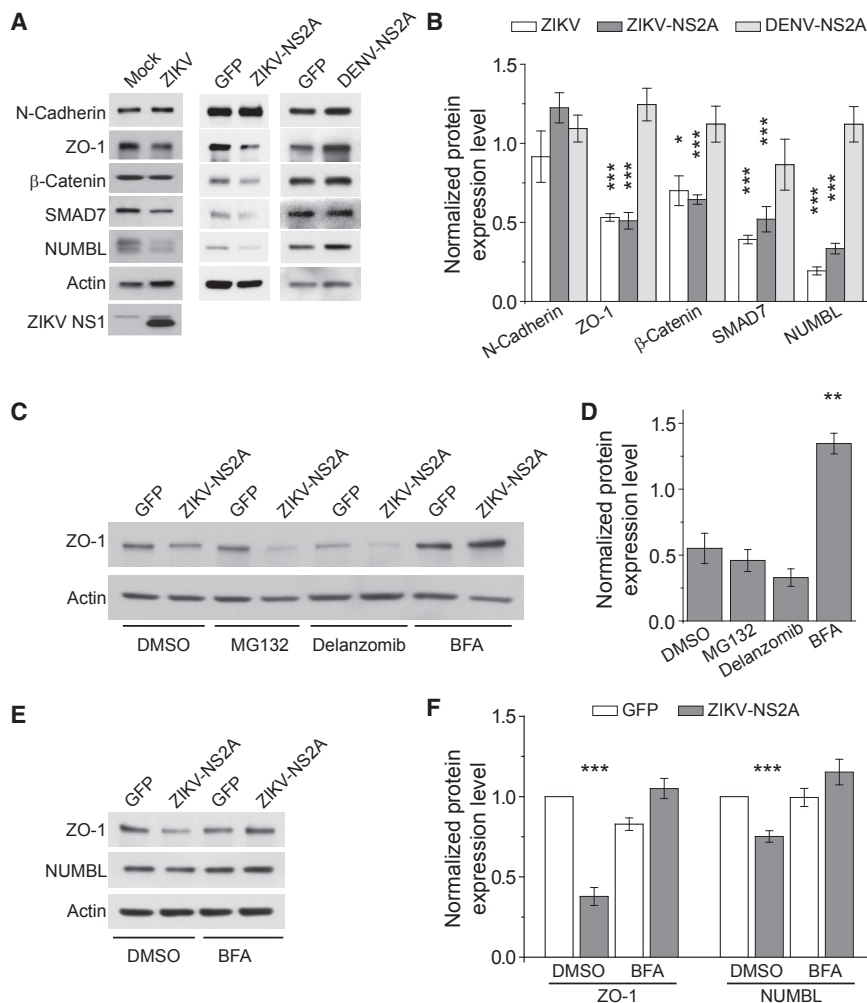


Figure 4. ZIKV-NS2A, but Not DENV-NS2A, Expression Leads to Adherens Junction Complex Component Degradation

(A and B) Sample western blot images of expression levels of adherens junction complex components in mouse neural progenitors infected with ZIKV, expressing ZIKV-NS2A, or expressing DENV-NS2A (A) and quantifications (B). Data were normalized to that of mock infection for the ZIKV infection condition or to that of GFP expression alone for the ZIKV-NS2A or DENV-NS2A conditions. Values represent mean \pm SEM ($n = 3$ cultures; $***p < 0.001$; $*p < 0.05$; Student's t test). (C and D) Sample western blot images of expression levels of ZO-1 upon 24 hr treatment of DMSO, MG-132 (20 μ M), delanzomib (60 nM), and BFA (100 nM) in HEK293 cells expressing GFP and ZIKV-NS2A or GFP alone (C) and quantifications (D). Data were first normalized to actin expression levels and then to the data from expression of GFP alone. Values represent mean \pm SEM ($n = 3$ cultures; $**p < 0.01$; Student's t test).

(E and F) Sample western blot images of expression levels of ZO-1 and NUMBL upon 24 hr treatment of DMSO or BFA (100 nM) of mouse cortical neural progenitors expressing GFP and ZIKV-NS2A or GFP alone (E) and quantifications (F). Data were normalized to that of actin. Values represent mean \pm SEM ($n = 3$ cultures; $***p < 0.001$; Student's t test).

Also see Figure S4.

results are reminiscent of a recent observation of AJ formation deficits, ventricular protrusions, and disorganized radial glia scaffolding in postmortem forebrain tissue of the first reported ZIKV-infected microcephalic fetus from an infected mother (Onorati et al., 2016).

DISCUSSION

The ZIKV epidemic and its association with microcephaly present a serious public health challenge. Understanding mechanisms underlying ZIKV pathogenesis in the developing mammalian brain may reveal potential targets for anti-ZIKV and neuroprotective therapeutic interventions. Our systematic and functional screen of ZIKV-encoded proteins led to the identification of an *in vivo* mechanism and a direct link of a ZIKV component to specific host machinery that can explain, at least in part, ZIKV-induced neural stem cell deficits during mammalian cortical neurogenesis *in vivo*. Our study also revealed additional deficits during cortical development that occurs after the early phases of neurogenesis, specifically in layer-specific positioning of newborn neurons in the developing cortex. Given the recent clinical findings that babies born to women infected with ZIKV during pregnancy

develop significant postnatal neurological deficits, such as epilepsy (Besnard et al., 2016; Moura da Silva et al., 2016; Sarno et al., 2016), our finding has important implications for future studies.

Our study revealed two potential cellular mechanisms by which ZIKV-NS2A reduces neural stem cell numbers in the developing cortex *in vivo* by reducing proliferation and through premature differentiation and depletion of RGCs. Previous studies in monolayer and 3D organoid cultures and in mice have already shown that ZIKV infection leads to reduced proliferation of neural progenitor cells (Ming et al., 2016). A recent study also showed that ZIKV infection of human brain organoids leads to premature differentiation of neural progenitors (Gabriel et al., 2017). Here, we identified ZIKV-NS2A protein, but not DENV-NS2A, as capable of mimicking, at least in part, the effect of direct ZIKV infection both in mice *in vivo* and in human forebrain organoids. Mechanistically, ZIKV-NS2A, but not DENV-NS2A, interacts with AJ complex components, and its expression leads to degradation of AJ complex components in neural progenitors and deficits in AJ formation of RGCs *in vivo*. Deficits in AJ formation have been shown to lead to aberrations in niche signaling that impact cortical neurogenesis (Stocker and Chenn, 2015). Additional deficits in radial glial fiber scaffolding may explain the positional defects of newborn neurons. Notably, two other flaviviruses, West Nile virus and Japanese encephalitis virus, also interact with AJ proteins and target junction proteins for lysosomal degradation in non-neuronal cells via viral

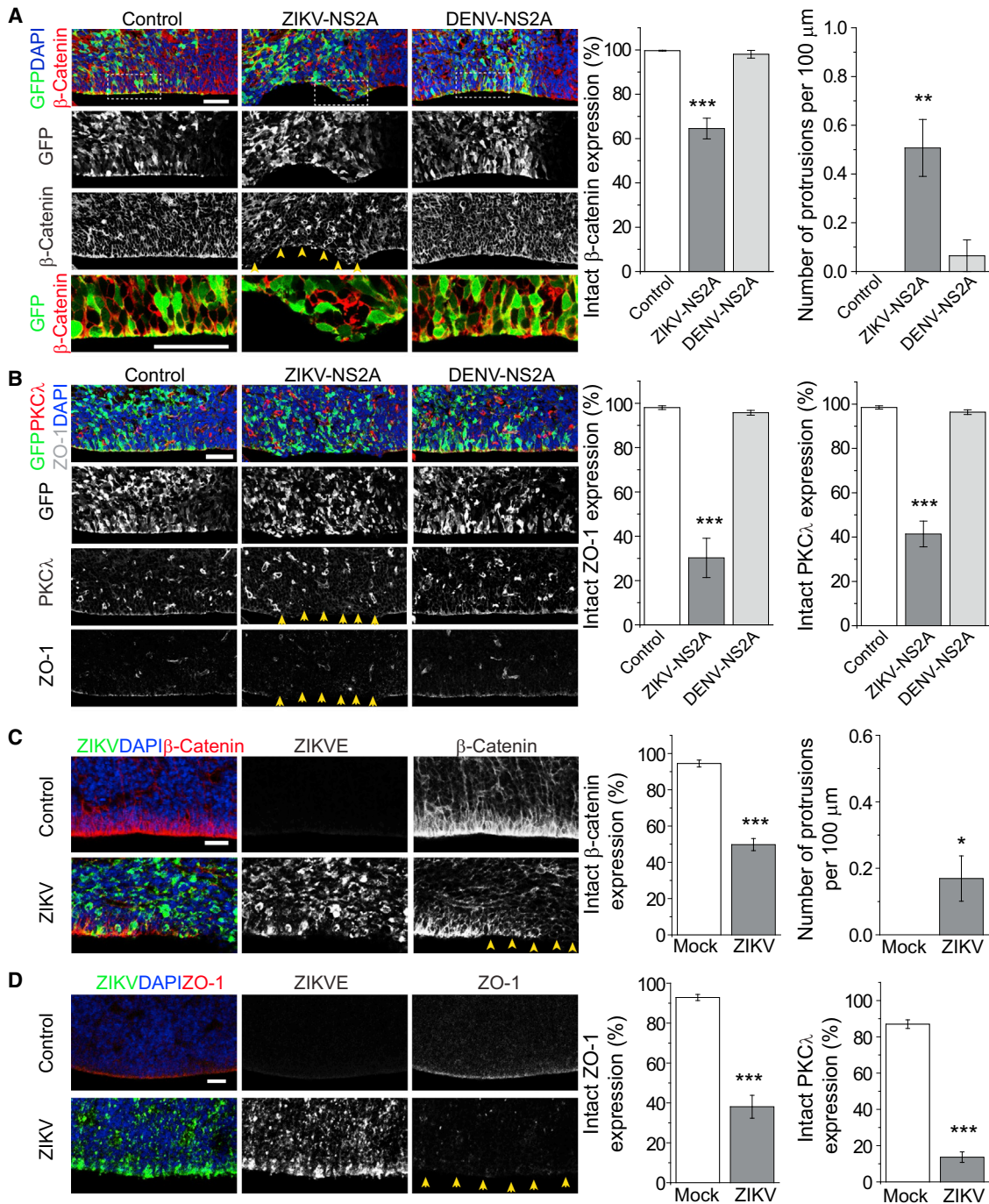


Figure 5. ZIKV-NS2A Expression and Direct ZIKV Infection Disrupt the Formation of Adherens Junction Complex in the Embryonic Mouse Cortex

(A and B) Embryonic mouse brains were electroporated at E14.5 to express GFP, GFP and ZIKV-NS2A, or GFP and DENV-NS2A and analyzed at E17.5. Sample confocal images of immunostaining for GFP, β -catenin (A), or PKC λ and ZO-1 (B) and staining for DAPI under different conditions are shown (left panels). The scale bars represent 50 μm . Arrows point to regions with discontinuous AJ formation. Regions in white boxes in (A) are shown at a higher magnification (bottom panels). Quantifications of continuous AJ formation and number of protrusions are also shown (right panels). Values represent mean \pm SEM (n = 5 sections from 3 animals; ***p < 0.001; **p < 0.01; Student's t test).

(C and D) ZIKV-SZ strain was injected into lateral ventricles of E13.5/E14.5 mice. Similar to (A) and (B), sample confocal images of immunostaining for ZIKV, β -catenin, and ZO-1 and staining for DAPI at E18.5 (left panels) and quantifications of continuous AJ formation at E18.5 and ventricular protrusions at P3 (right panels) are shown. Values represent mean \pm SEM (n = 6 sections from 4 animals; ***p < 0.001; *p < 0.05; Student's t test).

Also see Figure S5.

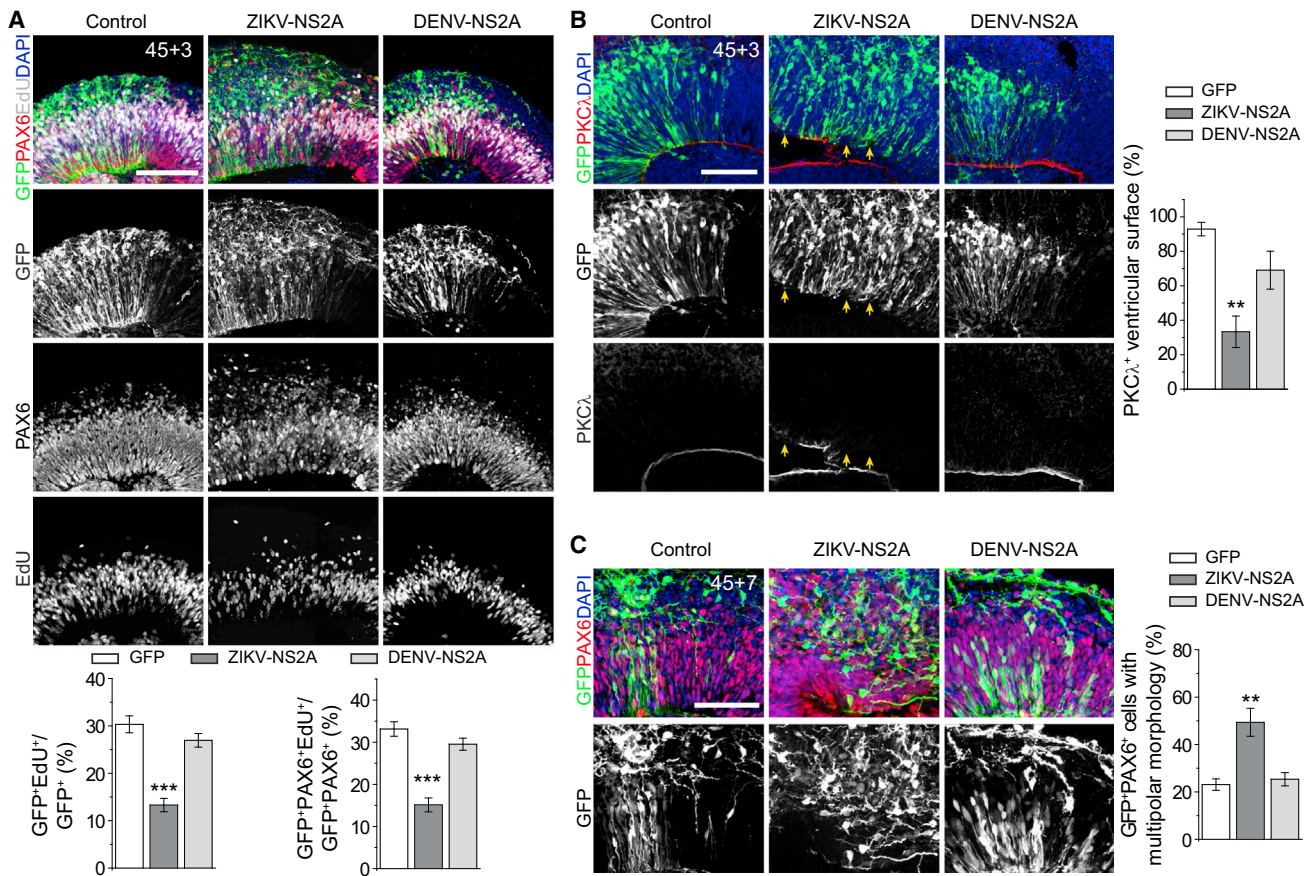


Figure 6. Expression of ZIKV-NS2A, but Not DENV-NS2A, Reduces Proliferation and Disrupts Adherens Junction Formation of Ventricular Radial Glial Cells in Human Forebrain Organoids

(A) Day 45 forebrain organoids were electroporated to express GFP, GFP and ZIKV-NS2A, or GFP and DENV-NS2A and analyzed 3 days later (45+3) after pulsing with EdU (10 μ M) for 1 hr. Sample confocal images for immunostaining for GFP and PAX6 and staining for EdU and DAPI are shown (top panels). Images represent cropped areas of tiled images that were acquired and automatically stitched with Zen software. The scale bar represents 100 μ m. Quantifications of percentages of EdU⁺GFP⁺ cells among all GFP⁺ cells or GFP⁺PAX6⁺EdU⁺ cells among GFP⁺PAX6⁺ cells are also shown (bottom panels). Values represent mean \pm SEM (n = 10 organoids; ***p < 0.001; Student's t test).

(B) Sample confocal images of immunostaining for GFP, PKC λ , and staining for DAPI are shown (left panels). Images represent cropped areas of tiled images that were acquired and automatically stitched with Zen software. The scale bar represents 100 μ m. Arrows point to regions with discontinuous AJ formation. Quantifications of AJ continuity based on PKC λ expression are also shown (right panel). Values represent mean \pm SEM (n = 9 organoids; **p < 0.01; Student's t test).

(C) Expression of ZIKV-NS2A, but not DENV-NS2A, or GFP alone led to a loss of typical radial glia morphology of PAX6⁺GFP⁺ cells at 7 days after electroporation (45+7). Sample confocal images of immunostaining for GFP and PAX6 and staining for DAPI (left panels; scale bar: 100 μ m) and quantification of percentages of GFP⁺PAX6⁺ cells with multipolar morphologies are shown. Values represent mean \pm SEM (n = 7 organoids; **p < 0.01; Student's t test).

Also see [Figure S6](#).

proteins different from NS2A (Agrawal et al., 2013; Medigeschi et al., 2009). It will be useful in the future to engineer ZIKVs with NS2A mutations that have high infection capacity but with no impact on neural stem cells to test how our identified mechanism contributes to the overall pathological impact of ZIKV on cortical neurogenesis. Given the tropism of ZIKV toward neural stem cells, these engineered viral vectors can be developed to target and manipulate radial glial cells in both fetal and adult mouse brains in vivo and in human brain organoids (Ming et al., 2016). Our finding does not rule out the possibility that interactions between ZIKV-NS2A and other host molecules may additionally regulate neural stem cell behavior. Our datasets of NS2A protein-protein interaction networks across the

human proteome provide a rich resource for future exploration. This global protein interactome may also be useful for understanding ZIKV/DENV replication and assembly to identify antiviral therapeutic targets. It is possible that other ZIKV components, including both ZIKV-encoded proteins (e.g., ZIKV-C; Liang et al., 2016) and noncoding RNAs (Pyro et al., 2016), may also contribute to the microcephaly phenotype observed in human fetuses and in animal models. Here, we provide an experimental paradigm that combines in vivo analysis of mouse cortical neural stem cells and in vitro analysis of human forebrain organoids to address basic mechanisms regulating mammalian cortical neurogenesis under normal and pathological conditions.

STAR★METHODS

Detailed methods are provided in the online version of this paper and include the following:

- **KEY RESOURCES TABLE**
- **CONTACT FOR REAGENT AND RESOURCE SHARING**
- **EXPERIMENTAL MODEL AND SUBJECT DETAILS**
 - Animals
 - HEK293 and primary mouse neural progenitor cells
 - Human iPSC lines
- **METHOD DETAILS**
 - DNA constructs
 - In utero electroporation
 - ZIKV infection of embryonic mice and analysis
 - Immunohistology and confocal imaging
 - NS2A in vitro binding assay
 - Cell culture, transfection and infection
 - CoIP and western blot analysis
 - RNA preparation and quantitative PCR
 - Forebrain organoid culture
 - Forebrain organoid electroporation
- **QUANTIFICATION AND STATISTICAL ANALYSES**
 - Analyses of mouse cortical neurogenesis
 - Statistical analysis on forebrain organoids

SUPPLEMENTAL INFORMATION

Supplemental Information includes six figures and four tables and can be found with this article online at <http://dx.doi.org/10.1016/j.stem.2017.07.014>.

AUTHOR CONTRIBUTIONS

K.-J.Y. led the project and was involved in all aspects of the study. G.S., J.P., H.-S.R., J.Q., and H.Z. performed protein array analysis. X.Q. and F.J. performed human organoid study. E.M.L. and H.T. performed viral infection. D.X., C.L., L.Y., C.-F.Q., Q.W., and Z.X. performed mouse ZIKV infection experiments. N.-S.K., C.H., F.Z., L.Z., W.-K.H., F.R.R., C.V., K.K., S.K., J.Y., Y.C., S.L., Z.W., K.M.C., and P.J. contributed to additional data collection and writing. K.-J.Y., H.S., and G.M. designed the project, analyzed the data, and wrote the paper.

ACKNOWLEDGMENTS

We thank members of Ming and Song laboratories for suggestions, L. Liu and Y. Cai for technical support, J. Schnoll for manuscript editing, and Dr. Park for help with statistical analysis. This work was supported by NIH grants R35NS097370 and R01MH105128 (G.M.), U19AI131130 (G.M., H.T., P.J., and Z.W.), R37NS047344 (H.S.), U19MH106434 (G.M., J.Q., and H.S.), P01NS097206 (H.S., J.Q., and P.J.), R01GM111514 (H.Z. and J.Q.), R25NS065729 and K12NS098482 (C.H.), and AI119530 (H.T.); the Simons Foundation (SFARI grant 308988 to H.S.); the Maryland Stem Cell Research Fund (MSCRF) (G.M. and H.S.); start-up funding from Emory (Z.W.); start-up funding from IGDB of CAS (Q.W.); China NSF (31430037) and the MOST “973” program (2014CB942801 and 2012YQ03026006 to D.X. and Z.X.); and Zika seed funding from Florida State University (H.T.). K.-J.Y. was supported by a postdoctoral fellowship from MSCRF and by a Young Investigator Award from Brain & Behavior Research Foundation. C.V. was partially supported by an NSF fellowship and T32GM007445.

Received: April 12, 2017

Revised: June 1, 2017

Accepted: July 21, 2017

Published: August 17, 2017

REFERENCES

- Agrawal, T., Sharvani, V., Nair, D., and Medigeshi, G.R. (2013). Japanese encephalitis virus disrupts cell-cell junctions and affects the epithelial permeability barrier functions. *PLoS ONE* 8, e69465.
- Besnard, M., Eyrolle-Guignot, D., Guillemette-Artur, P., Lastère, S., Bost-Bezeaud, F., Marcelis, L., Abadie, V., Garel, C., Moutard, M.L., Jouannic, J.M., et al. (2016). Congenital cerebral malformations and dysfunction in fetuses and newborns following the 2013 to 2014 Zika virus epidemic in French Polynesia. *Euro Surveill.* 27, pii: 30181.
- Braut, J.B., Khou, C., Basset, J., Coquand, L., Fraissier, V., Frenkiel, M.P., Goud, B., Manuguerra, J.C., Pardigon, N., and Baffet, A.D. (2016). Comparative analysis between flaviviruses reveals specific neural stem cell tropism for Zika virus in the mouse developing neocortex. *EBioMedicine* 10, 71–76.
- Buchman, J.J., and Tsai, L.H. (2007). Spindle regulation in neural precursors of flies and mammals. *Nat. Rev. Neurosci.* 8, 89–100.
- Chen, Y.T., Stewart, D.B., and Nelson, W.J. (1999). Coupling assembly of the E-cadherin/beta-catenin complex to efficient endoplasmic reticulum exit and basal-lateral membrane targeting of E-cadherin in polarized MDCK cells. *J. Cell Biol.* 144, 687–699.
- Chiang, C.H., Su, Y., Wen, Z., Yoritomo, N., Ross, C.A., Margolis, R.L., Song, H., and Ming, G.L. (2011). Integration-free induced pluripotent stem cells derived from schizophrenia patients with a DISC1 mutation. *Mol. Psychiatry* 16, 358–360.
- Cugola, F.R., Fernandes, I.R., Russo, F.B., Freitas, B.C., Dias, J.L., Guimarães, K.P., Benazzato, C., Almeida, N., Pignatari, G.C., Romero, S., et al. (2016). The Brazilian Zika virus strain causes birth defects in experimental models. *Nature* 534, 267–271.
- Currle, D.S., Hu, J.S., Kolski-Andreaco, A., and Monuki, E.S. (2007). Culture of mouse neural stem cell precursors. *J. Vis. Exp.* 2007, 152.
- Driggers, R.W., Ho, C.Y., Korhonen, E.M., Kuivanen, S., Jääskeläinen, A.J., Smura, T., Rosenberg, A., Hill, D.A., DeBiasi, R.L., Vezina, G., et al. (2016). Zika virus infection with prolonged maternal viremia and fetal brain abnormalities. *N. Engl. J. Med.* 374, 2142–2151.
- Gabriel, E., Ramani, A., Karow, U., Gottardo, M., Natarajan, K., Gooi, L.M., Goranci-Buzhala, G., Krut, O., Peters, F., Nikolic, M., et al. (2017). Recent Zika virus isolates induce premature differentiation of neural progenitors in human brain organoids. *Cell Stem Cell* 20, 397–406.e5.
- Garcez, P.P., Loiola, E.C., Madeiro da Costa, R., Higa, L.M., Trindade, P., Delvecchio, R., Nascimento, J.M., Brindeiro, R., Tanuri, A., and Rehen, S.K. (2016). Zika virus impairs growth in human neurospheres and brain organoids. *Science* 352, 816–818.
- Garcia-Blanco, M.A., Vasudevan, S.G., Bradrick, S.S., and Nichitta, C. (2016). Flavivirus RNA transactions from viral entry to genome replication. *Antiviral Res.* 134, 244–249.
- Giry-Laterrière, M., Verhoeven, E., and Salmon, P. (2011). Lentiviral vectors. *Methods Mol. Biol.* 737, 183–209.
- Götz, M., and Huttner, W.B. (2005). The cell biology of neurogenesis. *Nat. Rev. Mol. Cell Biol.* 6, 777–788.
- Heymann, D.L., Hodgson, A., Sall, A.A., Freedman, D.O., Staples, J.E., Althabe, F., Baruah, K., Mahmud, G., Kandun, N., Vasconcelos, P.F., et al. (2016). Zika virus and microcephaly: why is this situation a PHEIC? *Lancet* 387, 719–721.
- Hu, S., Wan, J., Su, Y., Song, Q., Zeng, Y., Nguyen, H.N., Shin, J., Cox, E., Rho, H.S., Woodard, C., et al. (2013). DNA methylation presents distinct binding sites for human transcription factors. *eLife* 2, e00726.
- Huang da, W., Sherman, B.T., and Lempicki, R.A. (2009). Systematic and integrative analysis of large gene lists using DAVID bioinformatics resources. *Nat. Protoc.* 4, 44–57.
- Jeong, J.S., Jiang, L., Albino, E., Marrero, J., Rho, H.S., Hu, J., Hu, S., Vera, C., Bayron-Poueymiroy, D., Rivera-Pacheco, Z.A., et al. (2012). Rapid identification of monospecific monoclonal antibodies using a human proteome microarray. *Mol. Cell Proteomics* 11, O111.016253.

- Li, C., Xu, D., Ye, Q., Hong, S., Jiang, Y., Liu, X., Zhang, N., Shi, L., Qin, C.F., and Xu, Z. (2016a). Zika virus disrupts neural progenitor development and leads to microcephaly in mice. *Cell Stem Cell* **19**, 120–126.
- Li, H., Saucedo-Cuevas, L., Shresta, S., and Gleeson, J.G. (2016b). The neurobiology of Zika virus. *Neuron* **92**, 949–958.
- Liang, Q., Luo, Z., Zeng, J., Chen, W., Foo, S.S., Lee, S.A., Ge, J., Wang, S., Goldman, S.A., Zlokovic, B.V., et al. (2016). Zika virus NS4A and NS4B proteins deregulate Akt-mTOR signaling in human fetal neural stem cells to inhibit neurogenesis and induce autophagy. *Cell Stem Cell* **19**, 663–671.
- Lindenbach, B.D., Thiel, H.J., and Rice, C.M. (2007). Flaviviridae: the viruses and their replication. In *Fields Virology*, D.M. Knipe and P.M. Howley, eds. (Philadelphia, PA, USA: Lippincott Williams and Wilkins), pp. 1101–1152.
- Ma, D.K., Chiang, C.H., Ponnusamy, K., Ming, G.L., and Song, H. (2008). G9a and Jhd2m2a regulate embryonic stem cell fusion-induced reprogramming of adult neural stem cells. *Stem Cells* **26**, 2131–2141.
- Matsuda, T., and Cepko, C.L. (2004). Electroporation and RNA interference in the rodent retina in vivo and in vitro. *Proc. Natl. Acad. Sci. USA* **101**, 16–22.
- Medigeshi, G.R., Hirsch, A.J., Brien, J.D., Uhrlaub, J.L., Mason, P.W., Wiley, C., Nikolich-Zugich, J., and Nelson, J.A. (2009). West Nile virus capsid degradation of claudin proteins disrupts epithelial barrier function. *J. Virol.* **83**, 6125–6134.
- Ming, G.L., Tang, H., and Song, H. (2016). Advances in Zika virus research: stem cell models, challenges, and opportunities. *Cell Stem Cell* **19**, 690–702.
- Mrakar, J., Korva, M., Tul, N., Popović, M., Poljšak-Prijatelj, M., Mraz, J., Kolenc, M., Resman Rus, K., Vesnaver Vipotnik, T., Fabjan Vodusek, V., et al. (2016). Zika virus associated with microcephaly. *N. Engl. J. Med.* **374**, 951–958.
- Moura da Silva, A.A., Ganz, J.S., Sousa, P.D., Doriqui, M.J., Ribeiro, M.R., Branco, M.D., Queiroz, R.C., Pacheco, M.J., Vieira da Costa, F.R., Silva, F.S., et al. (2016). Early growth and neurologic outcomes of infants with probable congenital Zika virus syndrome. *Emerg. Infect. Dis.* **22**, 1953–1956.
- Onorati, M., Li, Z., Liu, F., Sousa, A.M., Nakagawa, N., Li, M., Dell'Anno, M.T., Gulden, F.O., Pochareddy, S., Tebbenkamp, A.T., et al. (2016). Zika virus disrupts phospho-TBK1 localization and mitosis in human neuroepithelial stem cells and radial glia. *Cell Rep.* **16**, 2576–2592.
- Pylro, V.S., Oliveira, F.S., Morais, D.K., Cuadros-Orellana, S., Pais, F.S., Medeiros, J.D., Geraldo, J.A., Gilbert, J., Volpini, A.C., and Fernandes, G.R. (2016). ZIKV - CDB: a collaborative database to guide research linking SncRNAs and ZIKA virus disease symptoms. *PLoS Negl. Trop. Dis.* **10**, e0004817.
- Qian, X., Nguyen, H.N., Song, M.M., Hadiono, C., Ogden, S.C., Hammack, C., Yao, B., Hamersky, G.R., Jacob, F., Zhong, C., et al. (2016). Brain-region-specific organoids using mini-bioreactors for modeling ZIKV exposure. *Cell* **165**, 1238–1254.
- Rasin, M.R., Gazula, V.R., Breunig, J.J., Kwan, K.Y., Johnson, M.B., Liu-Chen, S., Li, H.S., Jan, L.Y., Jan, Y.N., Rakic, P., and Sestan, N. (2007). Numb and Numb1 are required for maintenance of cadherin-based adhesion and polarity of neural progenitors. *Nat. Neurosci.* **10**, 819–827.
- Rasmussen, S.A., Jamieson, D.J., Honein, M.A., and Petersen, L.R. (2016). Zika virus and birth defects—reviewing the evidence for causality. *N. Engl. J. Med.* **374**, 1981–1987.
- Sarno, M., Aquino, M., Pimentel, K., Cabral, R., Costa, G., Bastos, F., and Brites, C. (2016). Progressive lesions of central nervous system in microcephalic fetuses with suspected congenital Zika virus syndrome. *Ultrasound Obstet. Gynecol.* Published online September 19, 2016. <http://dx.doi.org/10.1002/uog.17303>.
- Shannon, P., Markiel, A., Ozier, O., Baliga, N.S., Wang, J.T., Ramage, D., Amin, N., Schwikowski, B., and Ideker, T. (2003). Cytoscape: a software environment for integrated models of biomolecular interaction networks. *Genome Res.* **13**, 2498–2504.
- Stocker, A.M., and Chenn, A. (2015). The role of adherens junctions in the developing neocortex. *Cell Adhes. Migr.* **9**, 167–174.
- Su, Y., Shin, J., Zhong, C., Wang, S., Roychowdhury, P., Lim, J., Kim, D., Ming, G.L., and Song, H. (2017). Neuronal activity modifies the chromatin accessibility landscape in the adult brain. *Nat. Neurosci.* **20**, 476–483.
- Szklarczyk, D., Franceschini, A., Wyder, S., Forslund, K., Heller, D., Huerta-Cepas, J., Simonovic, M., Roth, A., Santos, A., Tsafou, K.P., et al. (2015). STRING v10: protein-protein interaction networks, integrated over the tree of life. *Nucleic Acids Res.* **43**, D447–D452.
- Tang, H., Hammack, C., Ogden, S.C., Wen, Z., Qian, X., Li, Y., Yao, B., Shin, J., Zhang, F., Lee, E.M., et al. (2016). Zika virus infects human cortical neural progenitors and attenuates their growth. *Cell Stem Cell* **18**, 587–590.
- Wen, Z., Nguyen, H.N., Guo, Z., Lalli, M.A., Wang, X., Su, Y., Kim, N.S., Yoon, K.J., Shin, J., Zhang, C., et al. (2014). Synaptic dysregulation in a human iPSC cell model of mental disorders. *Nature* **515**, 414–418.
- Wen, Z., Song, H., and Ming, G.L. (2017). How does Zika virus cause microcephaly? *Genes Dev.* **31**, 849–861.
- Wu, K.Y., Zuo, G.L., Li, X.F., Ye, Q., Deng, Y.Q., Huang, X.Y., Cao, W.C., Qin, C.F., and Luo, Z.G. (2016). Vertical transmission of Zika virus targeting the radial glial cells affects cortex development of offspring mice. *Cell Res.* **26**, 645–654.
- Xu, M., Lee, E.M., Wen, Z., Cheng, Y., Huang, W.K., Qian, X., Tcw, J., Kouznetsova, J., Ogden, S.C., Hammack, C., et al. (2016). Identification of small-molecule inhibitors of Zika virus infection and induced neural cell death via a drug repurposing screen. *Nat. Med.* **22**, 1101–1107.
- Yoon, K.J., Nguyen, H.N., Ursini, G., Zhang, F., Kim, N.S., Wen, Z., Makri, G., Nauen, D., Shin, J.H., Park, Y., et al. (2014). Modeling a genetic risk for schizophrenia in iPSCs and mice reveals neural stem cell deficits associated with adherens junctions and polarity. *Cell Stem Cell* **15**, 79–91.
- Yoshimori, T., Yamamoto, A., Moriyama, Y., Futai, M., and Tashiro, Y. (1991). Bafilomycin A1, a specific inhibitor of vacuolar-type H(+)-ATPase, inhibits acidification and protein degradation in lysosomes of cultured cells. *J. Biol. Chem.* **266**, 17707–17712.
- Zhu, J., Liao, G., Shan, L., Zhang, J., Chen, M.R., Hayward, G.S., Hayward, S.D., Desai, P., and Zhu, H. (2009). Protein array identification of substrates of the Epstein-Barr virus protein kinase BGLF4. *J. Virol.* **83**, 5219–5231.

STAR★METHODS

KEY RESOURCES TABLE

REAGENT or RESOURCE	SOURCE	IDENTIFIER
Antibodies		
Rabbit anti-Pax6	BioLegend	PRB-278P, RRID: AB_2313780
Mouse anti-Pax6	BD Bioscience	561664, RRID: AB_10895587
Rabbit anti-Tbr2	Abcam	ab23345, RRID: AB_778267
Chicken anti-GFP	Aveslab	GFP-1020, RRID: AB_10000240
Mouse anti-Ki67	BD Bioscience	550609, RRID: AB_393778
Goat anti-Sox2	Santa Cruz	sc-17320, RRID: AB_2286684
Chicken anti-Nestin	Aveslab	NES, RRID: AB_2314882
Mouse anti-PKC λ	BD Bioscience	610207, RRID: AB_397606
Mouse anti-N-Cadherin	Innovative Research	18-0224, RRID: AB_86735
Rabbit anti-Actin	Cytoskeleton	AAN01, RRID: AB_10708070
Mouse anti- β -Catenin	BD Bioscience	610153, RRID: AB_397554
Rabbit anti-ZO-1	Thermo Fisher Scientific	40-2200, RRID: AB_10104693
Rabbit anti- Numb1	Abcam	ab37500, RRID: AB_881766
Rabbit anti-SMAD7	Thermo Fisher Scientific	42-0400, RRID: AB_2533512
Rabbit anti-ZIKV NS1	GeneTex	GTX133307
Goat anti-GFP	Rockland	600-101-215, RRID: AB_218182
Rabbit anti-Calnexin	Abcam	ab10286, RRID: AB_2069009
Human serum of ZIKV-infected patients	(Li et al., 2016a)	N/A
Chemicals, Peptides, and Recombinant Proteins		
ProLong Gold Antifade Mountant	Thermo Fisher Scientific	P10144
DAPI	Thermo Fisher Scientific	D1306, RRID: AB_2629482
StemPro Accutase Cell Dissociation Reagent	Thermo Fisher Scientific	A1110501
Matrigel Matrix	Corning	354277
SimplyBlue SafeStain	Thermo Fisher Scientific	LC6060
Y-27632	Cellagen Technology	C9127-2 s
EdU	Thermo Fisher Scientific	A10044
Phosphatase Inhibitor Cocktail	Cell Signaling	5870
Protease Inhibitor Cocktail	Sigma	P8340
4x Laemmli Sample Buffer	Bio-Rad	1610747
A83-01	StemCell Technologies	72022
Dorsomorphin	StemCell Technologies	72102
SB431542	StemCell Technologies	72232
CHIR99021	StemCell Technologies	72052
Dulbecco's Phosphate-Buffered Saline (DPBS)	Corning	21-031
Dulbecco's Modification of Eagle's Medium (DMEM)	Corning	10-013
DMEM/F-12, HEPES	GIBCO	11330-032
Neurobasal Medium	GIBCO	21103049
KnockOut Serum Replacement	GIBCO	10828028
GlutaMAX Supplement	GIBCO	35050061
MEM Non-Essential Amino Acids Solution	GIBCO	11140050
Penicillin-Streptomycin (10,000 U/mL)	GIBCO	15140122
2-Mercaptoethanol	GIBCO	21985023
N-2 Supplement	GIBCO	17502048
B-27 Supplement	GIBCO	17504044

(Continued on next page)

Continued

REAGENT or RESOURCE	SOURCE	IDENTIFIER
Matrigel Growth Factor Reduced (GFR) Basement Membrane Matrix	Corning	354230
Insulin solution	Sigma-Aldrich	I0516
Fetal Bovine Serum (FBS)	Corning	35-010
0.1% Gelatin in Water	StemCell Technologies	7903
Advanced DMEM/F-12	GIBCO	12634010
Human recombinant LIF	StemCell Technologies	78055
Compound E	StemCell Technologies	73952
MG-132	Cell Signaling	2194
Recombinant Human FGF-basic	Peptotech	100-18B
Recombinant Human EGF-basic	R&D Systems	P01133
Polybrene Infection/Transfection Reagent	Thermo Fisher Scientific	TR1003G
Bafilomycin A1	Sigma-Aldrich	B1793
Delanzomib	Kindly gifted by Dr. Wei Zheng (NIH/NCATS)	N/A
Critical Commercial Assays		
Click-iT EdU Assay Kits	Thermo Fisher Scientific	C10340
Cy5-NHS ester	GE Healthcare	PA15101
SuperScript III First-Strand Synthesis System	Thermo Fisher Scientific	18080051
Fast SYBR Green Master Mix	Thermo Fisher Scientific	4385610
Lipofectamine 2000	Thermo Fisher Scientific	11668027
Anti-HA Magnetic Beads	Thermo Fisher Scientific	88836
Endoplasmic Reticulum Isolation Kit	Sigma-Aldrich	ER0100
RNeasy Mini Kit	QIAGEN	74104
Experimental Models: Cell Lines		
HEK293	ATCC	CRL-1573, RRID:CVCL_0045
C12 (iPSC from normal human foreskin fibroblasts)	(Wen et al., 2014)	N/A
Experimental Models: Organisms/Strains		
Mouse: CrI:CD1(ICR)	Charles River Laboratory	RRID: IMSR_CRL:22
Mouse: CrI:CF188	Charles River Laboratory	RRID: IMSR_CRL:23
Yeast: Y258	Kindly gifted by Dr. Michael Snyder (Yale University)	N/A
Virus: ZIKV-MR766	ZeptoMetrix	0810521CF
Virus: ZIKV-SZ	(Li et al., 2016a)	N/A
Oligonucleotides		
Primers for ZIKV ORF cloning	See Table S1	N/A
Primers for Q-PCR analysis	See Table S1	N/A
Recombinant DNA		
pDONR221	Thermo Fisher Scientific	12536017
pCAG-GFP	(Matsuda and Cepko, 2004)	Addgene plasmid: 11150
pEGH-A	(Zhu et al., 2009)	N/A
pCWX-R4-DEST-R2-PG	(Giry-Laterrière et al., 2011)	Addgene plasmid: 45957
pENTR-L4-Ubi-L1R	(Giry-Laterrière et al., 2011)	Addgene plasmid: 45959
Software and Algorithms		
ImageJ	NIH	https://imagej.nih.gov/ij/
Imaris	Bitplane	http://www.bitplane.com/imaris/imaris
MATLAB	MathWorks	https://www.mathworks.com/products/matlab.html
STRING 10.0 database	(Szklarczyk et al., 2015)	http://string-db.org/

(Continued on next page)

Continued

REAGENT or RESOURCE	SOURCE	IDENTIFIER
DAVID 6.8	(Huang da et al., 2009)	https://david.ncifcrf.gov/
Zen	Zeiss	https://www.zeiss.com/microscopy/us/products/microscope-software/zen.html
Other		
SuperSignal West Dura Extended Duration Substrate	Thermo Fisher Scientific	34075
Costar 6 Well Clear Flat Bottom Ultra Low Attachment plate	Sigma-Aldrich	CLS3471
Nucleofector Kits for Mouse Neural Stem Cells	Lonza	VAPG-1004
Nucleofector 2b Device	Lonza	AAB-1001
Square wave electroporator	Nepa Gene	CUY21SC
Tweezers with platinum disk electrode	Nepa Gene	CUY650-5
Immun-Blot PVDF Membrane	Bio-Rad	1620177
12-well Spinning Bioreactor	(Qian et al., 2016)	N/A
LSM 800 confocal microscope	Zeiss	LSM 800
Leica CM3050S Research Cryostat	Leica Biosystems	CM3050S

CONTACT FOR REAGENT AND RESOURCE SHARING

Further information and requests for resources and reagents should be directed to and will be fulfilled by the Lead Contact, Guo-li Ming (gming@mail.med.upenn.edu). There are no restrictions on any data or materials presented in this paper.

EXPERIMENTAL MODEL AND SUBJECT DETAILS

Animals

All mice were housed with free access to food and water under pathogen-free conditions, in a facility where the temperature and light cycles (12 hr cycle) were controlled. All animal procedures used in this study were performed in accordance with the protocol approved by the Institutional Animal Care and Use Committee of Johns Hopkins University School of Medicine and by the Beijing Institute of Microbiology and Epidemiology Animal Care and Use Committee. All human studies followed IRB, ISCRO approved by John Hopkins University School of Medicine. Timed-pregnant Crl:CD1(ICR) mice (Charles River Laboratory) at E14.5 were used for in utero electroporation analysis. Pregnant ICR mice at E13.5/E14.5 were used for ZIKV infection.

HEK293 and primary mouse neural progenitor cells

HEK293 cells were obtained from ATCC and maintained in DMEM (GIBCO BRL), 10% FBS and Penicillin/Streptomycin (Invitrogen). Mouse NPCs were isolated from CD1 mouse embryonic cortices and cultured in Neurobasal medium (GIBCO BRL) containing 20 ng/ml FGF2, 20 ng/ml EGF, 5 mg/ml heparin, 2% B27 (v/v, GIBCO BRL), Glutamax (Invitrogen), Penicillin/Streptomycin (Invitrogen) on culture dishes pre-coated with Matrigel matrix (2%, Corning).

Human iPSC lines

The human iPSC line used in the current study (C1, male) was fully characterized (Wen et al., 2014; Yoon et al., 2014). They were cultured in stem cell medium, consisting of DMEM:F12 (Invitrogen) supplemented with 20% Knockout Serum Replacer (GIBCO), 1X Non-essential Amino Acids (Invitrogen), 1X Penicillin/Streptomycin (Invitrogen), 1X 2-Mercaptoethanol (Millipore), 1X Glutamax (Invitrogen), and 10 ng/ml FGF-2 (Peprotech). Culture medium was changed every day. Human iPSCs were passaged every week onto a new plate pre-seeded with irradiated CF1 mouse embryonic fibroblasts (Charles River Laboratory). All studies were performed under approved protocols of Johns Hopkins University School of Medicine.

METHOD DETAILS

DNA constructs

To clone ZIKV- and DENV-encoded ORFs, ZIKV MR766 (African strain) and DENV-1 (Hawaiian strain) were used to infect mosquito cells. One μ g of total RNA was converted to cDNA using Superscript III (Thermo Fisher Scientific) for PCR templates. The viral ORFs were constructed by RT-PCR-based cloning from cDNA into the Gateway Entry vector system. Primer sets were designed for amplifying the full-length ORFs and attB1 and attB2 sequences at the 5' ends of each primer were added to clone PCR amplicon into Gateway Entry vector pDONR221 (Thermo Fisher Scientific) by Gateway recombination (Table S1). Using the expression pEGH-A vector for expression and purification of N-terminal GST fusion protein, a stop codon (TAA) was added between attB2- and the

gene-specific reverse primer sequences in all primers. All entry clones were verified to be without any mutations at the amino acid sequences of all viral proteins by comparing to reference genome sequences of each viral strain. To express and purify individual viral proteins, sequence-verified Entry clones were cloned into a yeast expression vector pEGH-A. Verified clones were transformed to yeast strain Y258 that expresses GST fusion proteins under the control of the galactose-inducible GAL1 promoter.

To construct mammalian expression vectors under the control of the human Ubiquitin C promoter, sequence-verified entry clones were cloned into a lentiviral destination vector pCWX-R4-DEST-R2-PG (Addgene plasmid: 45957) by Gateway recombination reactions with pENTR-L4-Ubi-L1R (Addgene plasmid: 45959). To generate HA-tagged ZIKV-NS2A and DENV-NS2A expression vectors for biochemical analysis, the entry clones were amplified by PCR using 5' primers with attB1 sequence and 3' primers with HA-attB2 sequence and reinserted into pDONR221 and pCWX-R4-DEST-R2-PG, by the same Gateway recombination, to fuse the HA sequence into the C-terminal of NS2A ORFs. All of the final constructs were sequenced to confirm complete correspondence with original ORF sequences.

In utero electroporation

In utero electroporation was performed as described previously (Yoon et al., 2014). In brief, timed-pregnant CD1 mice (Charles River Laboratory) at E14.5 were anesthetized and the uterine horns were exposed and approximately 1 to 2 μ L of plasmid DNA, 0.5 μ g/ μ L pCAG-GFP (Addgene plasmid: 11150) and 2.5 μ g/ μ L a ZIKV ORF expression vector (without HA tag) or an empty lentiviral vector, was injected manually into the lateral ventricles of the embryos using a calibrated micropipette. Five pulses (40 V, 50 ms in duration with a 950 ms interval) were delivered across the uterus with two 5-mm electrode paddles (CUY650-5, Nepa Gene) positioned on either side of the head by a square wave electroporator (CUY21SC, Nepa Gene). After electroporation, the uterus was placed back in the abdominal cavity and the wound was sutured. Mouse embryos were injected with EdU (150 mg/kg of body weight, Thermo Fisher Scientific) 2 hr before sacrifice at E17.5. For the analysis of neuronal positioning, embryos were electroporated at E14.5 and analyzed at E19.5. All animal procedures were performed in accordance with the protocol approved by the Johns Hopkins Institutional Animal Care and Use Committee.

ZIKV infection of embryonic mice and analysis

The ZIKV-SZ strain (GenBank accession no: KU866423) was obtained from Beijing Institute of Microbiology and Epidemiology, China. ZIKV infection of embryonic animals was performed as previously described (Li et al., 2016a). Briefly, pregnant ICR mice at E13.5/E14.5 were anesthetized and dissected to expose the uterine horns, followed by microinjection of \sim 1 μ L of ZIKV (6.5×10^5 PFU/ml) or PBS into the lateral ventricles of embryos using a calibrated micropipette. After virus injection, the embryos were put back into the abdominal cavity and the incision in the dams was sutured. The brains of infected pups and their littermate controls were collected at E18.5 and P3 for further analysis. The tissues were fixed in 4% PFA overnight, dehydrated in 30% sucrose in PBS and embedded in OCT compound for cryostat sectioning. The brain sections were immunostained with human serum of ZIKV-infected patients (Li et al., 2016a) and antibodies against adherens junction markers (Table S1). The percentage of intact adherens junctions labeled by β -Catenin and ZO-1 along the ventricular surface and the density of ventricular protrusions were evaluated with ImageJ software.

Immunohistology and confocal imaging

For immunostaining of tissue sections, brains of embryos were fixed with 4% PFA in PBS overnight at 4°C. Brains were cryoprotected in 30% sucrose in PBS, embedded in OCT compound, and sectioned coronally (20 μ m-thickness) on a Leica CM3050S cryostat. For immunostaining of HEK293 cells, cells were fixed with 4% PFA in PBS for 20 min at 4°C. Brain sections and cells were blocked and permeabilized with the blocking solution (5% normal donkey serum, 3% Bovine serum albumin and 0.1% Triton X-100 in PBS) for 1 hr at room temperature, followed by incubation with primary antibodies diluted in the blocking solution at 4°C overnight. Secondary antibodies diluted in blocking solution were applied to the sections for 1 hr at room temperature. Nuclei were visualized by incubating for 10 min with 0.1 mg/ml 4,6-diamidino-2-phenylindole (DAPI; Sigma-Aldrich) in PBS. Stained sections were mounted with ProLong Gold anti-fade reagents (Thermo Fisher Scientific) and analyzed. All the antibodies used are listed in Key Resources Table.

NS2A in vitro binding assay

NS2A proteins were expressed as GST fusions in budding yeast, and purified using glutathione Sepharose affinity chromatography as described previously (Hu et al., 2013). On day one, each yeast strain containing the NS2A construct was inoculated in SC-URA media including glucose at 30°C, 200 rpm, overnight. On day two, primary seed cultures were inoculated in two 16 mL of SC-URA media including raffinose and incubated at 30°C, 90 rpm, overnight. On day three, the expression of individual viral proteins was induced by adding final 2% galactose to yeast cultures when the culture reached O.D. 0.9. Induced yeast cells were harvested after 6 hr incubation and stored at -80°C until the protein purification. For the initial protein purification step, Zirconia beads and lysis buffer including protease inhibitor cocktail (Roche) and reducing agent were immediately added to frozen pellets and yeast cells were mechanically lysed. Supernatant was incubated with glutathione beads in fresh plates for 2 hr at 4°C. The mixtures of glutathione beads and individual viral proteins were washed each three times under both high (500 mM NaCl)- and low (100 mM NaCl) - salt washing buffers including a protease inhibitor and reducing agent. For quality control of eluted proteins, all purified proteins were examined by SimplyBlue stain or anti-GST western blot analysis.

Each purified ZIKV-2A protein and DENV-NS2A protein was fluorescently labeled with Cy5-NHS ester using a commercial kit (GE Life Science) and diluted to a final concentration of 10 ng/ μ L in 200 μ L of 1 X TBST with 2% BSA. HuProt arrays (version III), comprised

of 20,240 individually purified full-length human proteins (Jeong et al., 2012), were first blocked with 1 X TBST with 2% BSA at room temperature for 2 hr. Each labeled NS2A protein was incubated on the blocked HuProt arrays in duplicate at RT for 1 hr. After three 15 min washes with 1 X TBST, the HuProt arrays were briefly rinsed with water and dried. After scanning the HuProt arrays with a microarray scanner (GenePix 4000B), the NS2A binding signals were acquired and analyzed using the GenePix software.

GenePix 6.1 was used to align the spot-calling grid. For each protein spot, the median values of foreground (F_{ij}) and background (B_{ij}) intensities at site (i,j) on the microarray were extracted, respectively. The binding intensity (R_{ij}) of each protein spot was defined as F_{ij}/B_{ij} . Since each protein was printed in duplicate on each microarray, R_{ij} was averaged for the duplicate as R'_{ij} . Using a similar method as in our previous study (Hu et al., 2013), the Z-score of each probe was calculated based on the distribution of R'_{ij} ,

$$Z_{ij} = \frac{R'_{ij} - \bar{N}}{SD}$$

N is the mean signal value for all proteins on the protein array. A stringent cutoff ($Z \geq 10$) was used to determine the positive hit list (Table S2).

For protein-protein interaction analysis, the functional protein association network was constructed using STRING 10.0 database (Szklarczyk et al., 2015) (<http://string-db.org/>) (Table S3). The protein-protein interactions were obtained with the default parameters (confidence score 0.4). The P value of association enrichment was also given by the database taking all proteins in the protein microarray as background. The association network was generated using Cytoscape 3.2.1 (Shannon et al., 2003).

Gene ontology enrichment analyses for NS2A binding proteins were performed using DAVID 6.8 (<https://david.ncicrf.gov/>) (Huang et al., 2009). Compared to all proteins in the protein microarray, enriched terms for NS2A binding proteins (P value < 0.05) were listed (Table S4).

Cell culture, transfection and infection

HEK293 cells were cultured in DMEM containing 10% FBS (Hyclone, Logan, UT, USA), 4 mM L-glutamine (GIBCO BRL), 100 IU/ml penicillin (GIBCO BRL) and 100 μ g/ml streptomycin (GIBCO BRL). For co-immunoprecipitation experiments, HEK293 cells were transfected with control, ZIKV-NS2A-HA, and DENV-NS2A-HA expressing constructs with Lipofectamine 2000 (Thermo Fisher Scientific) and collected after 48 hr.

Mouse neural progenitors were isolated from E11.5 CD1 mouse embryos and cultured in Neurobasal medium (GIBCO BRL) containing 20 ng/ml FGF2, 20 ng/ml EGF, 5 mg/ml heparin, 2% B27 (v/v, GIBCO BRL), and 4 mM L-glutamine as previously described (Currie et al., 2007). High titer lentivirus was produced from HEK293 cells and used to infect mouse neural progenitors in the presence of 4 μ g/ml polybrene (Milipore) (Ma et al., 2008). Mouse neural progenitor lysates were collected 4 days after control, ZIKV-NS2A- or DENV-NS2A-expressing lentivirus for western blotting analysis. For coIP analysis, mouse neural progenitors were electroporated with empty lentiviral control vector or pCWX-ZIKV-NS2A-HA by Mouse neural stem cell nucleofactor kit (Lonza) and Nucleofector 2b Device (Lonza), and collected 3 days later. Mouse neural progenitors were infected with ZIKV MR766 at MOI 0.08 for 64 hr and collected for western blotting and quantitative PCR analysis (Tang et al., 2016).

CoIP and western blot analysis

For coIP analysis, HEK293 cells were homogenized in the lysis buffer containing Phosphate-buffered saline (pH 7.4), 1.5% Triton X-100, 1 mM Na_3VO_4 , 1 mM NaF, 1 mM DTT, and protease inhibitor cocktails (Sigma-Aldrich). The lysates were incubated for 15 min on ice, sonicated and centrifuged for 15 min at $15,000 \times g$ 4°C. The supernatants were collected and immunoprecipitated with anti-HA magnetic beads (Thermo Fisher Scientific) overnight at 4°C. The beads were thoroughly washed with lysis buffer, boiled with Laemmli Sample Buffer (Bio-Rad) and subjected to western blot analysis. For western blotting, samples were separated by 4%–20% SDS-PAGE, transferred to PVDF membranes (Bio-Rad), incubated with primary and secondary antibodies and visualized with SuperSignal West Dura Chemiluminescent Substrate (Thermo Fisher Scientific). Primary antibodies are listed in Key Resource Table. Quantification of bands was performed using ImageJ software.

Rough endoplasmic reticulum (RER) fractions were isolated from mouse neural progenitors after 4 days of control, ZIKV-NS2A- and DENV-NS2A-expressing lentivirus infection, using Endoplasmic Reticulum Isolation Kit (Sigma-Aldrich) according to the manufacturer's protocol. Two 100 mm dishes of mouse neural progenitors were homogenized and RER-enriched microsomes were precipitated by calcium chloride, solubilized by Laemmli Sample Buffer (Bio-Rad) and subjected to western blot analysis.

RNA preparation and quantitative PCR

For gene expression analysis, the total RNA fraction was immediately isolated from cultured mouse neural progenitor samples with RNeasy Mini Kit (QIAGEN), treated with DNaseI and reverse-transcribed into the first-strand cDNA with SuperScript III (Thermo Fisher Scientific) (Su et al., 2017). cDNAs were used for SYBR-green based quantitative real-time PCR to measure the expression level of target genes with the comparative CT method (ABI) (Su et al., 2017). The primers used for quantitative PCR are listed in Table S1.

Forebrain organoid culture

Human iPSC lines from healthy subjects used in the current study have been fully characterized (Chiang et al., 2011; Wen et al., 2014). Protocols for generation of forebrain organoids using the Spin Ω bioreactor were detailed previously (Qian et al., 2016). Briefly, human iPSCs were cultured in stem cell medium, consisting of DMEM:F12 (Invitrogen) supplemented with 20% Knockout Serum Replacer

(GIBCO), 1X Non-essential Amino Acids (Invitrogen), 1X Penicillin/Streptomycin (Invitrogen), 1X 2-Mercaptoethanol (Millipore), 1X Glutamax (Invitrogen), and 10 ng/ml FGF-2 (Peprotech) on irradiated CF1 mouse embryonic fibroblasts (Charles River). On day 1, iPSC colonies were detached by treatment of 1 mg/ml Collagenase Type IV (Invitrogen) for 1 hr and transferred to an Ultra-Low attachment 6-well plate (Corning Costar), containing 3 mL of stem cell medium (without FGF-2), plus 2 μ M Dorsomorphine (Sigma) and 2 μ M A83-01 (Tocris). On days 5-6, half of the medium was replaced with the induction medium consisting of DMEM:F12, 1X N2 Supplement (Invitrogen), 1X Penicillin/Streptomycin, 1X Non-essential Amino Acids, 1X Glutamax, 1 μ M CHIR99021 (Cellagentech), and 1 μ M SB-431542 (Cellagentech). On day 7, organoids were embedded in Matrigel (Corning) and continued to grow in the induction medium for 6 more days. On day 14, embedded organoids were mechanically dissociated from Matrigel and transferred to each well of a 12-well spinning bioreactor (Spin Ω) containing differentiation medium, consisting of DMEM:F12, 1X N2 and B27 Supplements (Invitrogen), 1X Penicillin/Streptomycin, 1X 2-Mercaptoethanol, 1X Non-essential Amino Acids, and 2.5 μ g/ml Insulin (Sigma).

Forebrain organoid electroporation

On day 45, forebrain organoids were transferred into PBS solution in a 10 cm petri dish for electroporation. A mixture of 0.5 μ L of plasmid DNA and 0.05% Fast green was injected into the ventricle-like cavity of neural tube structures in the forebrain organoid using a calibrated micropipette. About 3-4 locations on one side of each forebrain organoid were targeted by the injection. The DNA-injected side of the organoid was placed toward the positive electrode in the middle of 5 mm gap of electrode paddles (CUY650-5, Nepa Gene). Five pulses (40 V, 50 ms in duration with a 950 ms interval) were delivered by a square wave electroporator (CUY21SC, Nepa Gene). After electroporation, organoids were transferred back to Spin Ω bioreactor for continued culturing. On day 48 (45+3) or day 52 (45+7), organoids were pulsed by 10 μ M EdU (ThermoFisher) for 1 hr by directly adding EdU into culture media and fixed for immunostaining analysis (Qian et al., 2016).

QUANTIFICATION AND STATISTICAL ANALYSES

No statistical methods were used to pre-determine sample sizes but our sample sizes are similar to those generally employed previously (Qian et al., 2016; Yoon et al., 2014). No randomization or blinding was employed. Data in figure panels reflect several independent experiments performed on different days. Different statistical tests were performed as listed in figure legends.

Analyses of mouse cortical neurogenesis

For quantitative analysis of electroporated neocortices, only GFP⁺ cells localized within the dorsolateral cortex were examined. 3x3 tiled images were obtained to cover the electroporated region of each coronal section with a 20x or 40x objective by scanning microscope (Zeiss LSM 800) and compared with equivalent sections in littermate counterparts. Quantifications were performed using Imaris software (Bitplane). In detail, for quantification of cell proliferation and cell fate, GFP⁺ cells were marked, and GFP⁺Pax6⁺, GFP⁺Tbr2⁺, GFP⁺EdU⁺, GFP⁺Pax6⁺EdU⁺, and GFP⁺Tuj1⁺ cells were defined and counted based on the intensity of Pax6, Tbr2, Tuj1 and EdU immunofluorescence in GFP⁺ cells measured with the same criteria among different groups. For quantifications of β -Catenin, PKC λ , or ZO-1 expression and distribution, the total length of the GFP⁺ apical membrane and the total length of the β -Catenin⁺, PKC λ ⁺, or ZO-1⁺ apical membrane on the ventricular surface were measured by ImageJ software and % of intact expression of the total electroporated region was calculated. For quantification of the number of ventricular protrusions, bulged cell clusters more than 15 μ m away from the ventricular surface in DAPI stained images were defined and counted as ventricular protrusions. The average number of ventricular protrusions in 100 μ m length of the GFP⁺ apical membrane was calculated. All quantifications were performed with 4-7 brain sections from at least 3 animals. Data are presented as the mean \pm SEM and statistical significance was assessed using unpaired Student's t test and One-way ANOVA. For distribution plots of neuronal positioning, the distances between GFP⁺SATB2⁺ or GFP⁺CTIP2⁺ cells and the ventricular surface were calculated and plotted after dividing each distance by the total thickness of the neocortex. For statistical analysis, the normalized mean distance to the ventricular surface was determined for each section, an equal number of sections was used for each condition and the mean of mean distances was compared for each condition using unpaired Student's t test. Quantification was performed with eight brain sections from four animals.

Statistical analysis on forebrain organoids

For quantification after electroporation, randomly selected ventricular structures with electroporated "fan-shaped" regions facing toward the pial surface, but not the interior of organoid, were imaged by confocal microscope (Zeiss LSM 800). 2x3 or 2x2 tiled images were automatically stitched using 10% overlap between tiles by Zen software (Zeiss). Among electroporated cells labeled by GFP, EdU⁺, Ki67⁺ or PAX6⁺ nuclei were counted using ImageJ software, and the effect from expression of different constructs (GFP, GFP and ZIKV-NS2A, or GFP and DENV-NS2A) was evaluated by the percentage of EdU⁺ or Ki67⁺ cells among total GFP⁺ or GFP⁺PAX6⁺ cells. For analysis of AJ continuity, the length of PKC λ laminated ventricular surface was measured using ImageJ software, and divided by the total length of ventricular surface in the electroporated region. A ratio above 80% was defined as continuous AJ. For analysis of cell morphology, GFP⁺PAX6⁺ cells with 3 or more processes were defined as having multi-polar morphology, as opposed to bi-polar radial glia cells with a basal and an apical process. The effect from the expression of different constructs was evaluated by the percentage of multi-polar cells among total GFP⁺PAX6⁺ cells. Multiple organoids were quantified and Student's t test was used for statistical analysis.